Glycolytic metabolism and differentiation remodeling of hematopoietic stem cells in lung cancer

Ziqi Guo
Guangxi Normal University
Shiming Pu
Guangxi Normal University
Liu Yang
Guangxi Normal University
Yaping Liu
Guangxi Normal University
Xin Li
Guangxi Normal University
Hongxia Zhao
Guangxi Normal University
Zuping Zhou
Guangxi Normal University
Cheng Yang (yang_cheng1016@163.com)
Guangxi Normal University https://orcid.org/0000-0002-6969-1968

Research Article

Keywords:

Posted Date: November 4th, 2022

DOI: https://doi.org/10.21203/rs.3.rs-2201060/v1

Abstract

Objective

Lung cancer may be accompanied by the abnormal activity of hematopoietic stem cells (HSCs), which rapidly proliferate and are biased toward myeloid differentiation, leading to abnormal immune cell development and consequently tumor immune disorders. However, the mechanism underlying the altered behavioral function of HSCs in the tumor state remains unclear.

Methods

Meanwhile, glucose metabolism, which plays an important role in the self-renewal and differentiation of HSCs, is remodeled in lung carcinogenesis. The goal of this study was to examine the relationship between glucose metabolism and the abnormal activity of HSCs in a tumor environment. A LLC mouse model of lung cancer was established. Metabolomics assays were used to analyze the differences of metabolites and the metabolic pathways between HSCs of normal (N-HSCs) and tumor-bearing mice (T-HSCs).

Results

Pyruvate metabolic changes were observed the most. T-HSCs exhibited up-regulated oxidative phosphorylation, elevated mitochondrial number and activity, ATP and ROS levels. Injection of the gluconeogenesis inhibitor 2-DG into tumor-bearing mice resulted in altered proliferation and apoptosis of HSCs, reduced differentiation of myeloid cells, and decreased the myeloid-derived suppressor cells.

Conclusions

The present results suggest that glucose metabolic state in HSCs is altered during tumorigenesis. Glucose metabolism remodeling in tumor HSCs could change their differentiation preferences.

Introduction

Lung cancer is the main cause of cancer-related deaths worldwide. Surgery is often the preferred treatment for patients with lung cancer; some others are administered chemotherapy and targeted therapy post-surgery(1). While there have been a few advances in lung cancer treatment, the prognosis remains poor. As researchers gain a better understanding of the pathophysiology of lung cancer, several new therapeutic strategies have been proposed, such as immune checkpoint modulation and vaccine therapy(2). Clinical trials show that immunotherapy can afford better overall survival than previous approaches in lung cancer patients(3). Myeloid-derived suppressor cells (MDSCs), a heterogeneous population of cells, including myeloid progenitor cells, immature granulocytes, immature macrophages,

and immature dendritic cells, play a key role in immunosuppression in tumor state(4, 5). Under pathological conditions, such as tumor development, myeloid-derived precursor cells are unable to mature and remain at various stages of differentiation, transforming into MDSCs with immunosuppressive functions(6). MDSCs strongly inhibit the anti-tumor immune response by $CD4^+$ T cells, $CD8^+$ T cells, and natural killer cells in tumor patients, thereby promoting tumor progression(7). Currently, the proposed immunotherapeutic strategies for targeting lung cancer MDSCs include promoting the differentiation of MDSCs, blocking their inhibitory effects, or elimination the cells by using some chemical treatment and antibodies(5, 8). In addition, there is limited research focusing on the origin of MDSCs to nip the increase in their numbers in the bud.

All immune cells in the body, including MDSCs, develop from hematopoietic stem cells (HSCs) in the bone marrow, and HSCs have the ability of long-term self-renewal and the potential to differentiate into various types of mature immune cells. HSCs remain dormant as long-term HSC (LT-HSC), which helps increase the resilience and viability of HSCs(9). In contrast, Wu et al. found that during tumorigenesis (e.g., lung, liver, gastric, and cervical cancers), HSCs are abnormally activated; their ability to self-renew, mobilize, and exhibit homing is altered; and the number of myeloid progenitor cells, GMPs, precursor cells of MDSCs, in peripheral blood is dramatically increased (9–11). The relative abundance of HSCs and GMPs in the peripheral blood of patients with solid tumors has increased dramatically, and their richness is strongly correlated with tumor progression and patient prognosis(11–13). HSCs are located at the top of the immune cell differentiation pyramid, generating numerous functionally distinct monopotent progenitor cells and "terminally differentiated" cells through stepwise differentiation. During this process, the differentiation potential of the cells gradually decreases. However, Faiyaz N. et al. expressed that the differentiation of immune cells was not progressive and their fate may be determined in HSCs, without going through an intermediate differentiation process. Molecules associated with differentiation are already actively expressed in LT-HSCs(14). Naik et al. observed the differentiation of single lymphocyte progenitors (LMPPs) downstream of HSCs and their sister cells and found that all these cells differentiated into dendritic cells, as if they were imprinted with the same "brand"(15). Sanjuan et al. found that thrombo poietin induces HSCs to produce a subpopulation biased towards differentiation into platelets; this subpopulation induces platelet production(16). Therefore, HSCs may respond differently when the environment is subjected to distinctive stimuli, leading to changes in the type of downstream immune cell differentiation, further affecting the development of diseases. In an atherosclerosis mouse model, an abnormally active nervous system reduces CXCL12 expression in the bone marrow, which accelerates HSC proliferation and favors myeloid differentiation, producing more neutrophils and monocytes. These cells, through circulation, reach the nervous system and promote plaque inflammation(17). The hypothesis is that HSCs are not only associated with immune cell development but also participate directly in eliciting immune responses. HSCs, the origin of the immune system, may be aberrantly activated during tumorigenesis and progression, leading to the abnormal differentiation of downstream mature immune cells (e.g., MDSCs), promoting tumor progression.

In recent years, a large number of studies have found that the metabolic reprogramming of HSCs affects their proliferation, survival, and differentiation, and the level of glucose metabolism is closely connected with HSC status(18). Among the many pathways of cellular metabolism, aerobic glycolysis promotes the maintenance of dormant and primed HSCs, and oxidative phosphorylation (OXPHOS) increases significantly with cell differentiation(19). Interrupting or reducing the glycolysis process impairs the stemness of LT-HSCs, leading to the loss of their self-renewal potential(20, 21). Altering the expression of key enzymes of glucose metabolism can affect HSC functions such as dormancy, differentiation, and bone marrow graft reconstruction(22, 23). Pyruvate dehydrogenase kinase (*Pdk*) is a downstream gene of *Hif-α* and a key enzyme in the glucose metabolism pathway. *Pdk* helps HSCs maintain their resting state and apoptotic functions by inhibiting mitochondrial metabolism and the cell cycle. In double knockout *Pdk2* and *Pdk4* mice, the cell cycle in HSCs was activated and produced fewer erythrocytes. LT-HSCs from $Pdk2^{-/-}$:$Pdk4^{-/-}$ mice are defective in repopulation after transplantation(24). Tumor suppressor protein kinase (*Lkb1*) regulates cell proliferation and energy metabolism. *Lkb1*knockdown induces anemia in mice and causes a decrease in the proportion of myeloid cells(25, 26). On the other hand, alteration of key genes associated with the function of HSCs can also alter their metabolism. Deletion of *Cited2*, an important gene that regulates the resting and apoptotic functions of HSCs, increased the ROS and mitochondrial activity of HSCs and decreased the expression of the key genes of metabolism, *Pdk2* and *Pdk4*(27). In addition, under pathological conditions, such as aging and tumor development, HSCs change their cellular state to resist extrinsic stimuli through metabolic reprogramming(28–30). Ioannis M. et al. found that β-glucan altered the level of glucose metabolism and cholesterol synthesis in mice, inducing expansion of HSCs and generating more myeloid cells. Immune training of mice using β-glucan allows them to better cope with secondary infections and protects them against chemotherapy-induced bone marrow ablation(31). Thus, we hypothesized that there was an interactive relationship between the function and metabolism of HSCs, and that modulating the metabolism of tumor-HSCs might alter their function and downstream differentiation preferences.

Our study showed that glucose metabolism in HSCs was dramatically altered in the LLC lung cancer mouse model, leading to up-regulation of OXPHOS, elevated mitochondrial number and activity, altered expression of metabolic key enzyme genes, and increased ATP and reactive oxygen species (ROS) levels. In addition, the modulation of glucose metabolic remodeling in HSCs of tumor-bearing mice affected their cell differentiation, with a decrease in the number of MDSCs. Thus, it is possible to influence the type of immune cell differentiation by altering glucose metabolism in HSCs. Our study will improve our understanding of the metabolic change patterns and regulatory mechanisms of HSCs in tumor states and lay the theoretical foundation for tumor immunotherapeutic approaches based on the metabolic intervention of HSCs.

Materials And Methods

Animals

Female 2–3-month-old C57BL/6J mice were purchased from Laboratory Animal Resources, Chinese Academy of Sciences (Beijing, China) and housed in the Key Laboratory of Stem Cell and Pharmaceutical biotechnology of Guangxi Normal University. All animal care and procedures were approved by the Institutional Animal Care Committee.

Isolation and purification of HSCs

Four weeks after LLC cell inoculation, mice were executed and bone marrow monocyte suspensions were isolated and prepared. HSCs were analyzed or sorted by flow cytometry (FACS) by adding specific fluorescent labeling antibodies (Lin-eFluor450, CD150-PerCP-eFluor710, Sca-1-PE-Cy7, CD48-APC, CD117-APC-eFluor780, (BD, USA) and incubated for 30 min at 4°C. HSCs were harvested using Flow tubes containing 2 mL of DMEM complete medium.

Metabolomic analysis

FACS-sorted HSCs were washed twice with pre-cooled PBS; cellular primary metabolites were determined by GC-MS. Differences in the primary metabolites of HSCs from normal/tumor-bearing mice were compared by principal component analysis (PCA), differential metabolite analysis, heat map analysis, and pathway analysis, and their associated metabolic pathways were detected.

Analysis of ROS and membrane potential

For measurement of intracellular ROS levels, cells were incubated at 37°C in the dark for 20 min with 10 mM dichlorodihydrofluorescein diacetate (DCFDA; Invitrogen, USA) and analyzed using FACS.

HSCs were incubated with surface antibody for 30 min at 4°C and protected from light; 100 N tetramethylrhodamine methyl ester (TMRM; Immuno Chemistry Technologies, USA) was added and mixed by inverting several times. After incubation, the cells were centrifuged at 600 g for 4 min at 4°C. The supernatant was removed, and the mitochondrial membrane potential was detected using FACS.

Analysis of mitochondrial mass

Bone marrow cells from mice were collected, made into single-cell suspensions, added with prepared antibodies (Lin-FITC, CD150-PerCP-eFluor710, Sca-1-PE-Cy7, CD48-APC-eFluor780, CD117-PE-eFluor610), mixed by gentle blowing, incubated at 4°C, and kept in the dark for 30 min. Then subjected to Mito Tracker Deep Red (Cell signaling, Shanghai, China; 200 nM, pre-warmed at 37°C), incubated for 30 min at 37°C, protected from light, and analyzed using FACS.

Forimmunofluorescence staining analysis of mitochondrial mass, the sorted HSCs were collected and incubated with 5×10^4 cells/well in a 24-well plate. When the cells grew to the required density (80% confluent cultivation), the medium was aspirated, and Mito Tracker Deep Red (500 nM) pre-warmed at 37°C was added for staining. After staining, a fixative (methanol/glacial acetic acid, 3/1) was added for 10 min at -20°C. DAPI (100 μL, 15 μg/mL per well) solution was added and incubated for 15 min at 28°C, protected from light. An antifluorescence quenching blocker was added and the stained cells were observed using an inverted microscope.

Analysis of HSC lactate production

The sorted HSCs were collected and inoculated in 96-well plates at 1×10^4 cells/well, and the supernatants of cultured cells were collected for 24 hours of in vitro culture recovery. Culture supernatants were then analyzed using the Lactate Assay Kit (Abcam, UK) following the manufacturer's instructions.

Determination of acetyl-coenzyme A

The sorted HSCs were collected, and the cell suspension was diluted with PBS to 1×10^6 cells/mL. The cells were disrupted, and the intracellular components were released by repeat cycles of freeze-thaw. Cells were centrifuged for 20 min at 1100 x g, and the supernatant was carefully collected. HSC acetyl coenzyme A was detected using an acetyl coenzyme AKit (Abcam, UK).

Measurement of glucose uptake and intracellular ATP levels

The sorted HSCs were collected and cultured at 1×10^4 cells/well in 96-well plates. After pretreatment of HSCs with glucose-free medium, 50 nM 2-NBDG (Invitrogen) was added and incubated for 30 min at 37°C. Antibodies to the surface markers of HSCs were added, and glucose uptake was measured by flow cytometry. Intracellular ATP level was measured using the Luciferase ATP Determination Kit (Sigma-Aldrich, USA) following the manufacturer's instructions.

Determination of NADH

The sorted HSCs were divided into two groups, and one group of cells was treated with 2 mM antimycin (AMA; Sigma-Aldrich, UK) for 5 min at room temperature; NADH fluorescence was detected by FACS (UV440/40 nm channel). The difference in NADH fluorescence obtained before and after AMA stimulation was the NADH accumulated through mitochondrial OXPHOS, reflecting the OXPHOS level.

Determination of mitochondrial DNA copy number

Total DNA of HSCs was extracted, and the mitochondrial DNA copy number was detected by qPCR. The target gene was COXII (mtDNA), and β-tubulin (nuclear DNA) was the internal reference.

Cell viability

The sorted HSCs were inoculated in 96-well plates at 2×10^3 cells/well, and 10 μL CCK8 (Beyotime, China) was added to each well. Cells were incubated at 37°C for 4 h, and absorbance was detected at 450 nm.

Apoptosis

The cells were resuspended in 100 μL 1× binding buffer and incubated with 5 μL Annex in V for 15 min at 28°C and protected from light. Cells were incubated for 5 min at room temperature after adding 5 μL of propidium iodide (PI) and were protected from light. Apoptosis was measured using FACS.

Analysis of cell abundance

The bone marrow and spleen of mice were excised and prepared into single-cell suspensions, and the bone marrow cells were incubated with surface antibodies to HSCs, surface antibodies to erythroid cells (Ter119-FITC), surface antibodies to myeloid cells (Gr-1-APC, CD11b-PE-Cy7), and surface antibodies to lymphocytes (CD3-APC, CD4-PE, CD8a-PE-Cy7, B220 - PerCP-Cy5.5). Spleen cells were incubated with erythroid cell surface antibody, myeloid cell surface antibody, lymphocyte surface antibody, and hematopoietic stem cell antibody. After incubation for 30 min at 4°C, protected from light, the cells were analyzed using FACS.

Statistical analysis

SPSS18.0 statistical software was used for one-way ANOVA and two-way ANOVA. Statistical results are presented as mean ± standard deviation (SD); *($p < 0.05$) and **($p < 0.01$) indicate significant difference.

Results

Reprogramming of glucose metabolism in hematopoietic stem cells in lung carcinogenesis

During tumorigenesis, the number of HSCs increases, proliferation is up-regulated, and more MDSCs are differentiated compared with that in normal physiological conditions(32–34). Metabolism plays an important role in the maintenance of the quiescence and activation and differentiation of HSCs. A metabolome analyses was used to detect the metabolic profile of HSCs in lung cancer and to answer if this metabolism regulates the function of HSCs. We established a mouse model of LLC lung cancer and after four weeks we sorted HSPCs (T-HSPCs), including long-term HSCs (LT-HSCs), short-term HSCs (ST-HSCs), and multilineage progenitors (MPPs), from their bone marrow for metabolomics assays. (Fig. 1A). Compared to the control group (N-HSPCs), the most significant changes in metabolites were associated with glucose metabolism, such as pyruvate, lactate, α-ketoglutarate, and glucose levels. Metabolic pathway enrichment analysis showed that the pyruvate metabolic pathway may be closely linked to the functional changes of HSPCs (Fig. 1B-C).

Considering pyruvate has many destinations, the rate of glycolysis and OXPHOS in HSCs was analyzed. The isolation of LT-HSCs from normal and tumor-bearing mice (N-HSCs, and T-HSCs), respectively, revealed that the glucose uptake ability of T-HSCs changed (Fig. 2A). Lactate levels in T-HSCs increased (Fig. 2B), suggesting glycolysis may be up-regulated. Both acetyl coenzyme A, which is the OXPHOS substrate, and ATP levels were elevated in T-HSCs (Fig. 2C-D). To determine changes in the mitochondrial OXPHOS in T-HSCs, antimycin A (AMA), a specific mitochondrial electron transport chain inhibitor, was added to the sorted HSCs and analyzed NADH levels after incubating the cells for 5 min at 28°C. In the presence of AMA, the accumulation of NADH in cells depends only on the mitochondrial OXPHOS. Therefore, NADH levels can indicate the state of mitochondrial respiration. NADH accumulation in T-HSCs increased after the addition of AMA, indicating up-regulated OXPHOS in T-HSCs (Fig. 2E-F).

Changes in mitochondrial activity of HSCs in lung cancer

OXPHOS occurs in the mitochondria, and the activation of mitochondria is directly linked to the up-regulated OXPHOS. As shown in Fig. 1, the number of molecules related to mitochondrial OXPHOS was increased in T-HSCs. The assumption was that the mitochondrial activity of T-HSCs was up-regulated. Mitochondrial fluorescent dyes were used to determine mitochondrial mass by FACS. The results revealed a higher number of mitochondria in T-HSCs than N-HSCs (Fig. 3A-B). The same results were obtained using immunofluorescence (Fig. 3C).

MMP and ROS production reflect the functional state of mitochondria. Changes in the MMP of HSCs were studied using atetramethylrhodamine ethyl ester (TMRE) fluorescent dye (Fig. 4A), and the MMP of T-HSCs was found to be elevated ($p < 0.05$); ROS production was likewise significantly increased ($p < 0.01$) (Fig. 4B). These results also indicate increased mitochondrial activity in T-HSCs. The changes in mitochondrial DNA copy number using qPCR are shown in Fig. 4C. These results showed that the mitochondrial DNA copy number was significantly up-regulated ($p < 0.01$), consistent with the increase in the number of intracellular mitochondria, indicating the number and activity of mitochondria in T-HSC was elevated.

Changes in HSCs of lung cancer under the effect of 2-DG

As the rate of OXPHOS was increased due to upregulation of glucose metabolism in T-HSCs, inhibition of glucose metabolism could affect its cellular function. 2-DG was injected into the mice via tail vein and HSCs were sorted from the bone marrow one week later using flow cytometry. The glucose metabolism inhibitor 2-DG had little effect on the number of N-HSCs but was able to considerably reduce the proportion of T-HSCs (Fig. 5A-B). In vitro viability results showed that 2-DG led to less proliferation (Fig. 5C) and decreased the apoptosis of T-HSCs (Fig. 5D-E). These results suggest that the regulation of glucose metabolism by 2-DG can affect the status and function of HSCs and reduce their activity. The mitochondrial mass of T-HSCs was reduced in the presence of 2-DG, indicating that 2-DG can reduce the mitochondrial activity of T-HSCs (Fig. 5F-G). Existing studies suggest that the type of terminally differentiated cells have been determined in HSCs, and the expansion and differentiation of HSCs are derived from specific subpopulations(35–37). CD150 was used to distinguish the subpopulations of HSCs biased towards lymphoid differentiation/homeostasis/myeloid differentiation (Ly-bi/Bala/My-bi HSCs) characterized as $Lin^{-}Sca\text{-}1^{+}c^{-}Kit^{+}CD34^{-}CD135^{-}CD150^{-}$, $Lin^{-}Sca\text{-}1^{+}c\text{-}Kit^{+}CD34^{-}CD135^{-}CD150^{low}$, and $Lin^{-}Sca\text{-}1^{+}c\text{-}Kit^{+}CD34^{-}CD135^{-}CD150^{+}$, respectively (Fig. 5H-I). The results showed that the proportion of subpopulations biased toward myeloid cells was higher in T-HSCs than in N-HSCs. In lung carcinogenesis, HSCs differentiated to produce myeloid cells. The proportion of subpopulations of HSCs biased toward myeloid cells in T-HSCs was reduced after the addition of 2-DG, suggesting 2-DG may inhibit the differentiation of HSCs toward myeloid cells.

Changes in the abundance of immune cells in the bone marrow of mice with lung cancer after 2-DG stimulation.

Lung carcinogenesis was associated with a significant increase in the number of MDSCs in the bone marrow, a decrease in the number of erythrocytes and $CD8^+$ T cells, and insignificant changes in the number of $CD4^+$ T cells and B cells. The number of erythrocytes increased on adding 2-DG (Fig. 6A); the trend was reversed for MDSCs, as 2-DG reduced the number of MDSCs in the bone marrow of mice with lung cancer (Fig. 6B). On treatment with 2-DG, the number of erythrocytes and MDSCs shifted to that observed in the normal group. There were no significant changes in the ratio of $CD4^+$ T cells, $CD8^+$ T cells, or B cells (Fig. 6C-E).

Changes in the abundance of immune cells in the spleen of lung cancer mice after 2-DG stimulation.

Treatment with 2-DG had a weak effect on spleen size (Fig. 7A). In the spleen, 2-DG had little effect on the erythrocyteratio in tumor mice (Fig. 7B), but it significantly abrogated the proportion of MDSCs (Fig. 7C-D), consistent with the results obtained from bone marrow. There was little effect on the ratio of $CD4^+$ T cells, $CD8^+$ T cells, and B cells (Fig. 7E-G). From these results, it is clear that 2-DG can alter the abundance of immune cells, especially the number of MDSCs, in lung cancer mice. The effect of 2-DG on MDSCs may arise from its ability to prevent the differentiation of T-HSCs into myeloid cells. However, further studies are needed to confirm this hypothesis.

Gene expression pattern of T-HSCs.

To further elucidate the effect of T-HSCs, the gene expression pattern of T-HSCs was compared with that of N-HSCs. The expression heat map showed 199 differentially expressed genes between the two cell subsets, including 44 up-regulated genes, such as Rcvrn, Vldlr,Gpr65, Car5b, and 155 down-regulated genes, such as Ccl6, Jchain, Mpo, Prss34, Mcpt8 (Fig. 8A). These genes were associated with the cell cycle, RNA degradation, and ribosome biogenesis (Fig. 8B-8C). The genes with the most significant changes in expression are listed in Fig. 8D. The microarray results were validated using qPCR (Fig. 8E). qPCR validation provides a concrete proof of concept of our microarray analysis. The expression of genes related to glucose metabolism, such as Ldhd, Pdk2, Lkb1, and Sirt7, were examined. The results were consistent with previous data, suggesting both glycolysis and OXPHOS may be up-regulated.

Discussion

Existing studies suggest that LT-HSCs rely more on glycolysis than OXPHOS for energy production. As cells continue to differentiate, the proportion of metabolism through OXPHOS gradually increases(21, 38).When subjected to stressful conditions, HSCs overcome the resting state and respond to the energy

demands of specific conditions through metabolic reprogramming(39, 40). In tumorigenesis, LT-HSCs undergo imbalanced differentiation, generating more PMN-MDSCs, thus promoting tumor progression and poor prognosis(11, 13).Whether the differentiated bias of HSCs is associated with metabolic reprogramming is still unknown. Our observations indicate that the metabolic preferences of LT-HSCs change during tumorigenesis from being more dependent on glycolysis to being metabolized by both OXPHOS and glycolysis. The effect of abnormal glucose metabolism, owing to tumorigenesis on the differentiation of LT-HSCs has also been demonstrated. By inhibiting glucose metabolism, the imbalance in the differentiation of LT-HSCs can be reversed, resulting in a decrease in the production of MDSCs.

The metabolomics analysis of purified LSKs indicated their metabolism in the tumor state was altered, with a substantial increase in pyruvate metabolism (Fig. 1). The pyruvate and lactate levels were increased in Tumor-LSK (T-LSKs), indicating that the glycolysis metabolism in T-HSCs was not diminished. However, there was an increase in acetyl-coenzyme A and NADH levels, an increment in mitochondrial mass and DNA copy, and an up-regulation of ROS and ATP levels (Fig. 2–3) in T-HSCs, suggesting that the rate of OXPHOS is also elevated in T-HSCs. Glycolysis and OXPHOS have a reciprocal relationship(41, 42). For example, AML cells are usually OXPHOS-dependent, with limited glycolysis capacity, and exhibit high mitochondrial potential(43, 44). However, our results show an increase in glycolysis and OXPHOS in T-HSCs. From the immunofluorescence results (Fig. 3), the number of cells labeled by Mito Tracker red in N-HSCs and T-HSCs was approximately the same. However, the mitochondrial mass was particularly increased in T-HSCs, indicating that only a fraction of T-HSCs had a marked change in mitochondrial potentials, and the metabolism of these cells switched from glycolysis to OXPHOS.OXPHOS could produce greater than 18-fold ATP than glycolysis(45), and T-HSCs showed a limited ability to produce ATP, proving that only a fraction of the cells underwent metabolic transition. The cell population that undergoes metabolic transformation in T-HSCs may also be functionally altered, leading to imbalanced differentiation.

Mitochondrial activity in HSCs is lower than that inmitochondria-directed progenitor cells(21, 46–48). Reduction in the mitochondrial mass is accompanied by a decrease in mitochondrial OXPHOS activity and membrane potential(49). The metabolic capacity of mitochondria is closely monitored by the mitochondrial unfolded protein response (UPR^{mt})(50, 51), which is one of the major quality control mechanisms for mitochondrial self-renewal. In homeostatic conditions, approximately 90% of hematopoietic stem cells exist in a resting state(52). When stimulated with cytokines, hematopoietic stem cells transitioned from a quiescent to proliferative state, with an increased mitochondrial mass of HSCs and up-regulated expression of mitochondrial chaperones and proteases, suggesting the activation of UPR^{mt}(50).SIRT7, one of the key elements of UPR^{mt}, protects the stress-challenged HSC pool by inhibiting mitochondrial biosynthesis(51).Sirt7 acts as an inhibitor of mitochondrial biosynthesis, and its low expression in T-HSCs may lead to a decline in UPR^{mt} thus increasing mitochondrial number. The UPR^{mt} may be reduced in T-HSCs, and thus an increased number of mitochondria and extent of OXPHOS may be observed in T-HSCs. Sirt7 was up-regulated in aged HSCs. Mitochondrial dysfunction and abnormal ROS

levels have been reported to be relevant to aging HSCs. Aged HSCs show some similarities to tumor HSCs. Further experiments are needed to test this hypothesis.

There is an imbalance in the differentiation of immune cells in patients with tumors, thus producing more MDSCs owing to metabolic and functional changes in HSCs. Tumor-bearing mice produced fewer MDSCs and more erythrocytes on being treated with 2-DG.However, MDSCs are also regulated by 2-DG. In triple-negative breast cancer, aerobic glycolysis controls the expression of tumor granulocyte colony-stimulating factor (G-CSF) and granulocyte-macrophage colony-stimulating factor (GM-CSF) and regulates the differentiation of MDSC, thus influencing tumor progression and prognosis(53). The decrease in the number of MDSCs in tumor-bearing mice after 2-DG stimulation was due to the changes in the differentiation of HSCs or as a direct result of treatment with 2-DG. CD150 was used to distinguish subpopulations of HSCs capable of distinguishing myeloid-bias from that capable of distinguishing lymphocyte-bias subpopulations of HSCs(37). After treatment with 2-DG, there was a decrease in myeloid-preferring HSCs, suggesting that the decrease in the number of downstream myeloid cells was a result of the change in HSCs differentiation preference. Leal Oburogluet al. found that 2-DG could improve erythroid lineage commitment and decrease myeloid lineage of HSCs in vitro(54), which is consistent with the results of this study—2-DG increased erythroid cells both in the bone marrow and spleen. In addition, in some diseases, 2-DG can influence the disease state by altering the metabolism of HSCs. Wei Du et al. suggested that metabolic reprogramming from glycolysis to OXPHOS is performed in Fanconi anemia (FA) HSCs through a p53-dependent mechanism in response to oxidative stress(40). 2-DG prominently reduced the number of HSCs in the bone marrow and reduced the repopulating ability of FA HSCs. Furrer et al. suggested that tumor-associated anemia is caused by a decrease in the viability of erythrocytes(55). Although our data showed that 2-DG restored erythrocytes in tumor-bearing mice, it is unclear whether 2-DG altered erythropoiesis or affected erythrocyte viability, for example, by inhibiting apoptosis. Thus, further studies are required to address this issue.

Conclusions

Together, our results demonstrate that T-HSCs undergo metabolic reprogramming from being solely glycolysis-dependent to becoming glycolysis- and OXPHOS-dependent. The differentiation preferences of HSCs changed during tumorigenesis, producing more MDSCs, thus promoting tumor progression and metastasis. Treatment with 2-DG alters glycolysis metabolism, cellular function, and differentiation preferences of T-HSCs, leading to a decrease in the number of MDSCs. Metabolic reprogramming of HSCs, which may alter the differentiation preferences of HSCs and decrease the production of cancer-promoting immune cells, might serve as a possible means to treat tumors in the future.

Declarations

Acknowledgements

Not applicable.

Author contributions

CY, ZG, and ZZ conceived the study and analyzed the data. YL and XL performed the experiments and drafted the manuscript. CY and ZZ obtained funding for the study and supervised the experiments. All authors read and approved the final manuscript.

Funding

This study was granted by the National Natural Science Foundation of China (32160159, 81972700 and 61827819) and National Science Foundation of Guangxi (2022GXNSFBA035546).

Availability of data and materials

The datasets used and/or analysed during the current study are available from the corresponding author on reasonable request.

Ethics approval and consent to participate

The animal experiments were in accordance with the Ethics Committee of Experimental Animals of Guangxi Normal University.

Consent for publication

Not applicable.

Competing interests

The authors declare that they have no competing interests.

Author details

[1]School of Life Sciences, Guangxi Normal University, Guilin 541004, China. [2]Guangxi Universities Key Laboratory of Stem Cell and Biopharmaceutical Technology, Guangxi Normal University, China. [3] Key Laboratory of Ecology of Rare and endangered Species and Environmental Protection, Guangxi Normal University, China. [4]Research Center for Biomedical Sciences, Guangxi Normal University, China. [5]Faculty of Biological and Environmental Science, University of Helsinki, Finland.

References

1. Siegel RL, Miller KD, Jemal A. Cancer statistics. 2015. CA: a cancer journal for clinicians. 2015;65(1):5–29.
2. Byron E, Pinder-Schenck M. Systemic and targeted therapies for early-stage lung cancer. Cancer control: journal of the Moffitt Cancer Center. 2014;21(1):21–31.

3. Hall RD, Gray JE, Chiappori AA. Beyond the standard of care: a review of novel immunotherapy trials for the treatment of lung cancer. Cancer control: journal of the Moffitt Cancer Center. 2013;20(1):22–31.
4. Gabrilovich DI, Nagaraj S. Myeloid-derived suppressor cells as regulators of the immune system. Nat Rev Immunol. 2009;9(3):162–74.
5. Ma J, Xu H, Wang S. Immunosuppressive Role of Myeloid-Derived Suppressor Cells and Therapeutic Targeting in Lung Cancer. J Immunol Res. 2018;2018:6319649.
6. Hargadon KM, Bullock TN. The role of tumor/dendritic cell interactions in the regulation of anti-tumor immunity: the good, the bad, and the ugly. Front Immunol. 2014;5:178.
7. Bronte V, Brandau S, Chen SH, Colombo MP, Frey AB, Greten TF, et al. Recommendations for myeloid-derived suppressor cell nomenclature and characterization standards. Nat Commun. 2016;7:12150.
8. Wang Y, Tian J, Wang S. The potential therapeutic role of myeloid-derived suppressor cells in autoimmune arthritis. Semin Arthritis Rheum. 2016;45(4):490–5.
9. Sahin E, Depinho RA. Linking functional decline of telomeres, mitochondria and stem cells during ageing. Nature. 2010;464(7288):520–8.
10. Kleppe M, Spitzer MH, Li S, Hill CE, Dong L, Papalexi E, et al. Jak1 Integrates Cytokine Sensing to Regulate Hematopoietic Stem Cell Function and Stress Hematopoiesis. Cell Stem Cell. 2018;22(2):277.
11. Wu WC, Sun HW, Chen HT, Liang J, Yu XJ, Wu C, et al. Circulating hematopoietic stem and progenitor cells are myeloid-biased in cancer patients. Proc Natl Acad Sci USA. 2014;111(11):4221–6.
12. Pu S, Qin B, He H, Zhan J, Wu Q, Zhang X, et al. Identification of early myeloid progenitors as immunosuppressive cells. Sci Rep. 2016;6:23115.
13. Netherby CS, Messmer MN, Burkard-Mandel L, Colligan S, Miller A, Cortes Gomez E, et al. The Granulocyte Progenitor Stage Is a Key Target of IRF8-Mediated Regulation of Myeloid-Derived Suppressor Cell Production. J Immunol. 2017;198(10):4129–39.
14. Notta F, Zandi S, Takayama N, Dobson S, Gan OI, Wilson G, et al. Distinct routes of lineage development reshape the human blood hierarchy across ontogeny. Science. 2016;351(6269):aab2116.
15. Naik SH, Perie L, Swart E, Gerlach C, van Rooij N, de Boer RJ, et al. Diverse and heritable lineage imprinting of early haematopoietic progenitors. Nature. 2013;496(7444):229–32.
16. Sanjuan-Pla A, Macaulay IC, Jensen CT, Woll PS, Luis TC, Mead A, et al. Platelet-biased stem cells reside at the apex of the haematopoietic stem-cell hierarchy. Nature. 2013;502(7470):232–6.
17. Heidt T, Sager HB, Courties G, Dutta P, Iwamoto Y, Zaltsman A, et al. Chronic variable stress activates hematopoietic stem cells. Nat Med. 2014;20(7):754–8.
18. Garcia-Prat L, Sousa-Victor P, Munoz-Canoves P. Proteostatic and Metabolic Control of Stemness. Cell Stem Cell. 2017;20(5):593–608.

19. Liang R, Arif T, Kalmykova S, Kasianov A, Lin M, Menon V, et al. Restraining Lysosomal Activity Preserves Hematopoietic Stem Cell Quiescence and Potency. Cell Stem Cell. 2020;26(3):359–76. e7.
20. Suda T, Takubo K, Semenza GL. Metabolic regulation of hematopoietic stem cells in the hypoxic niche. Cell Stem Cell. 2011;9(4):298–310.
21. Papa L, Djedaini M, Hoffman R. Mitochondrial Role in Stemness and Differentiation of Hematopoietic Stem Cells. Stem cells international. 2019;2019:4067162.
22. Kyoko I, Massimo B, Keisuke I. Metabolism as master of hematopoietic stem cell fate. Int J Hematol. 2018;109:18–27.
23. Papa L, Djedaini M, Hoffman R. Mitochondrial Role in Stemness and Differentiation of Hematopoietic Stem Cells. Stem cells international. 2019;2019:1–10.
24. Takubo K, Nagamatsu G, Kobayashi C, Nakamura-Ishizu A, Kobayashi H, Ikeda E, et al. Regulation of glycolysis by Pdk functions as a metabolic checkpoint for cell cycle quiescence in hematopoietic stem cells. Cell Stem Cell. 2013;12(1):49–61.
25. Nakada D, Saunders, Thomas L, Morrison, et al. Lkb1 regulates cell cycle and energy metabolism in haematopoietic stem cells. Nature. 2010.
26. Gan B, Hu J, Jiang S, Liu Y, Sahin E, Zhuang L, et al. Lkb1 regulates quiescence and metabolic homeostasis of haematopoietic stem cells. Nature.
27. Du J, Li Q, Tang F, Puchowitz MA, Fujioka H, Dunwoodie SL, et al. Cited2 is required for the maintenance of glycolytic metabolism in adult hematopoietic stem cells. Stem Cells & Development. 2014;23(2):83.
28. So WK, Cheung TH. Molecular Regulation of Cellular Quiescence: A Perspective from Adult Stem Cells and Its Niches. Methods Mol Biol. 2018;1686:1–25.
29. Ren R, Ocampo A, Liu GH, Izpisua Belmonte JC. Regulation of Stem Cell Aging by Metabolism and Epigenetics. Cell Metabol. 2017;26(3):460–74.
30. Ahlqvist KJ, Suomalainen A, Hamalainen RH. Stem cells, mitochondria and aging. Biochim Biophys Acta. 2015;1847(11):1380–6.
31. Mitroulis I, Ruppova K, Wang B, Chen LS, Grzybek M, Grinenko T, et al. Modulation of Myelopoiesis Progenitors Is an Integral Component of Trained Immunity. Cell. 2018;172(1–2):147 – 61 e12..
32. Mizukoshi E, Kaneko S. Immune cell therapy for hepatocellular carcinoma. J Hematol Oncol. 2019;12(1):52.
33. Dominguez D, Ye C, Geng Z, Chen S, Fan J, Qin L, et al. Exogenous IL-33 Restores Dendritic Cell Activation and Maturation in Established Cancer. J Immunol. 2017;198(3):1365–75.
34. Kustermann M, Klingspor M, Huber-Lang M, Debatin KM, Strauss G. Immunostimulatory functions of adoptively transferred MDSCs in experimental blunt chest trauma. Sci Rep. 2019;9(1):7992.
35. Challen GA, Boles NC, Chambers SM, Goodell MA. Distinct hematopoietic stem cell subtypes are differentially regulated by TGF-beta1. Cell Stem Cell. 2010;6(3):265–78.

36. Beerman I, Bhattacharya D, Zandi S, Sigvardsson M, Weissman IL, Bryder D, et al. Functionally distinct hematopoietic stem cells modulate hematopoietic lineage potential during aging by a mechanism of clonal expansion. Proc Natl Acad Sci USA. 2010;107(12):5465–70.
37. Liu Y, Van Zant G, Liang Y. Measuring the aging process in stem cells. Methods Mol Biol. 2015;1235:19–32.
38. Takubo K, Nagamatsu G, Kobayashi CI, Nakamura-Ishizu A, Kobayashi H, Ikeda E, et al. Regulation of glycolysis by Pdk functions as a metabolic checkpoint for cell cycle quiescence in hematopoietic stem cells. Cell Stem Cell. 2013;12(1):49–61.
39. Simsek T, Kocabas F, Zheng J, Deberardinis RJ, Mahmoud AI, Olson EN, et al. The distinct metabolic profile of hematopoietic stem cells reflects their location in a hypoxic niche. Cell Stem Cell. 2010;7(3):380–90.
40. Du W, Amarachintha S, Wilson AF, Pang Q. SCO2 Mediates Oxidative Stress-Induced Glycolysis to Oxidative Phosphorylation Switch in Hematopoietic Stem Cells. Stem Cells. 2016;34(4):960–71.
41. Huang X, Trinh T, Aljoufi A, Broxmeyer HE. Hypoxia Signaling Pathway in Stem Cell Regulation: Good and Evil. Curr Stem Cell Rep. 2018;4(2):149–57.
42. Mistry JJ, Marlein CR, Moore JA, Hellmich C, Wojtowicz EE, Smith JGW, et al. ROS-mediated PI3K activation drives mitochondrial transfer from stromal cells to hematopoietic stem cells in response to infection. Proc Natl Acad Sci USA. 2019;116(49):24610–9.
43. Shi L, Yan H, An S, Shen M, Jia W, Zhang R, et al. SIRT5-mediated deacetylation of LDHB promotes autophagy and tumorigenesis in colorectal cancer. Mol Oncol. 2019;13(2):358–75.
44. Jones CL, Stevens BM, D'Alessandro A, Reisz JA, Culp-Hill R, Nemkov T, et al. Inhibition of Amino Acid Metabolism Selectively Targets Human Leukemia Stem Cells. Cancer Cell. 2019;35(2):333–5.
45. Folmes CD, Dzeja PP, Nelson TJ, Terzic A. Metabolic plasticity in stem cell homeostasis and differentiation. Cell Stem Cell. 2012;11(5):596–606.
46. Maryanovich M, Zaltsman Y, Ruggiero A, Goldman A, Shachnai L, Zaidman SL, et al. An MTCH2 pathway repressing mitochondria metabolism regulates haematopoietic stem cell fate. Nat Commun. 2015;6:7901.
47. Papa L, Zimran E, Djedaini M, Ge Y, Ozbek U, Sebra R, et al. Ex vivo human HSC expansion requires coordination of cellular reprogramming with mitochondrial remodeling and p53 activation. Blood Adv. 2018;2(20):2766–79.
48. Ito K, Bonora M, Ito K. Metabolism as master of hematopoietic stem cell fate. Int J Hematol. 2019;109(1):18–27.
49. Ho TT, Warr MR, Adelman ER, Lansinger OM, Flach J, Verovskaya EV, et al. Autophagy maintains the metabolism and function of young and old stem cells. Nature. 2017;543(7644):205–10.
50. Mohrin M, Widjaja A, Liu Y, Luo H, Chen D. The mitochondrial unfolded protein response is activated upon hematopoietic stem cell exit from quiescence. Aging Cell. 2018;17(3):e12756.

51. Mohrin M, Shin J, Liu Y, Brown K, Luo H, Xi Y, et al. Stem cell aging. A mitochondrial UPR-mediated metabolic checkpoint regulates hematopoietic stem cell aging. Science. 2015;347(6228):1374–7.
52. Hao S, Chen C, Cheng T. Cell cycle regulation of hematopoietic stem or progenitor cells. Int J Hematol. 2016;103(5):487–97.
53. Li W, Tanikawa T, Kryczek I, Xia H, Li G, Wu K, et al. Aerobic Glycolysis Controls Myeloid-Derived Suppressor Cells and Tumor Immunity via a Specific CEBPB Isoform in Triple-Negative Breast Cancer. Cell Metabol. 2018;28(1):87–103. e6.
54. Oburoglu L, Tardito S, Fritz V, de Barros SC, Merida P, Craveiro M, et al. Glucose and glutamine metabolism regulate human hematopoietic stem cell lineage specification. Cell Stem Cell. 2014;15(2):169–84.
55. Furrer R, Jauch AJ, Nageswara Rao T, Dilbaz S, Rhein P, Steurer SA, et al. Remodeling of metabolism and inflammation by exercise ameliorates tumor-associated anemia. Sci Adv. 2021;7(37):eabi4852.

Figures

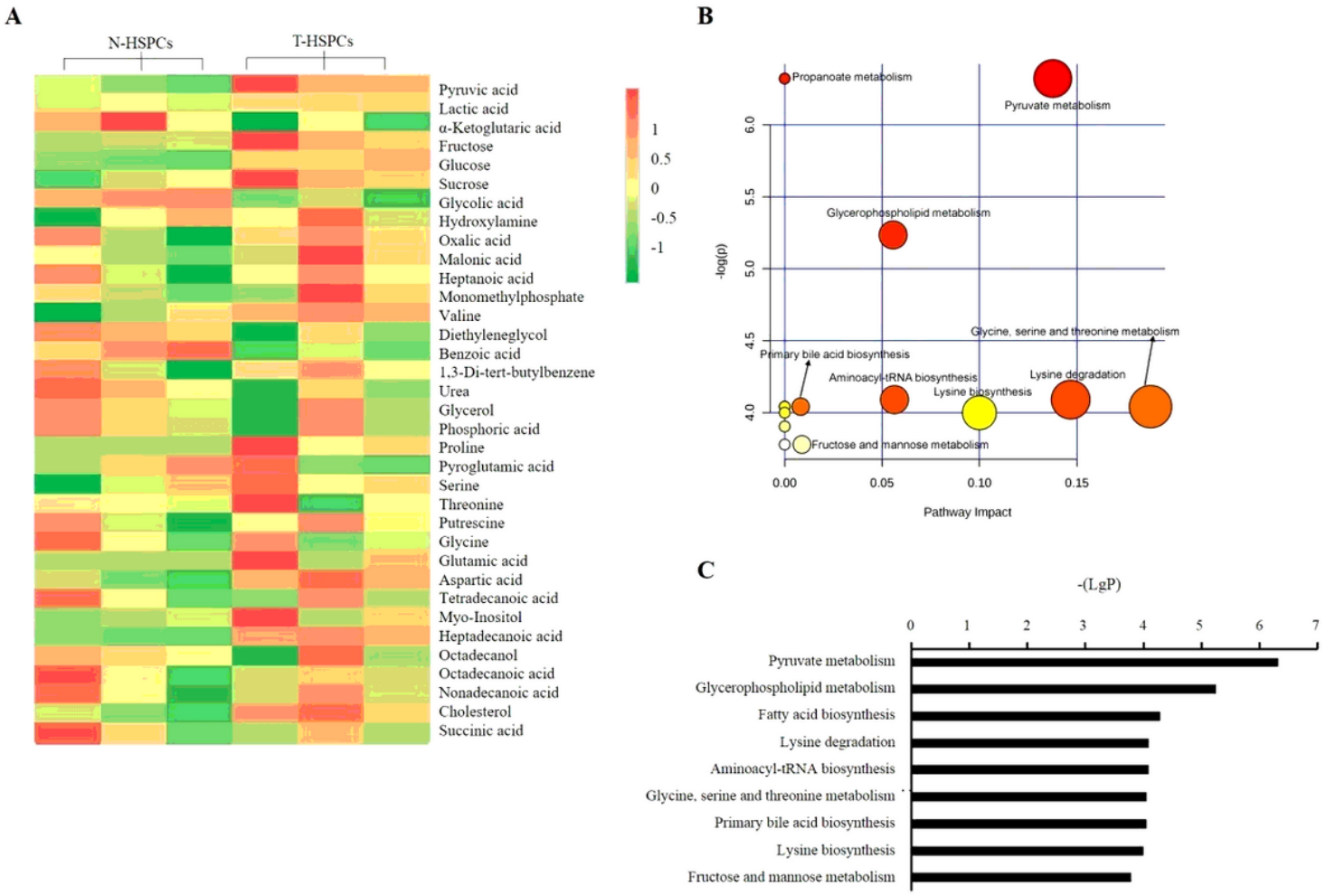

Figure 1

Metabolomic profiling of LSKs in Lung cancer. **(A)** Heat map of distinct metabolites. N-LSKs: LSKs isolated from bone marrow of normal mice, T-LSKs: LSKs isolated from bone marrow of tumor-bearing mice. **(B)** Metabolic pathway enrichment analysis. The larger the vertical coordinate, the more relevant the pathway is to the classification. **(C)** Overview of metabolites that were enriched in T-LSKs compared to N-LSKs.

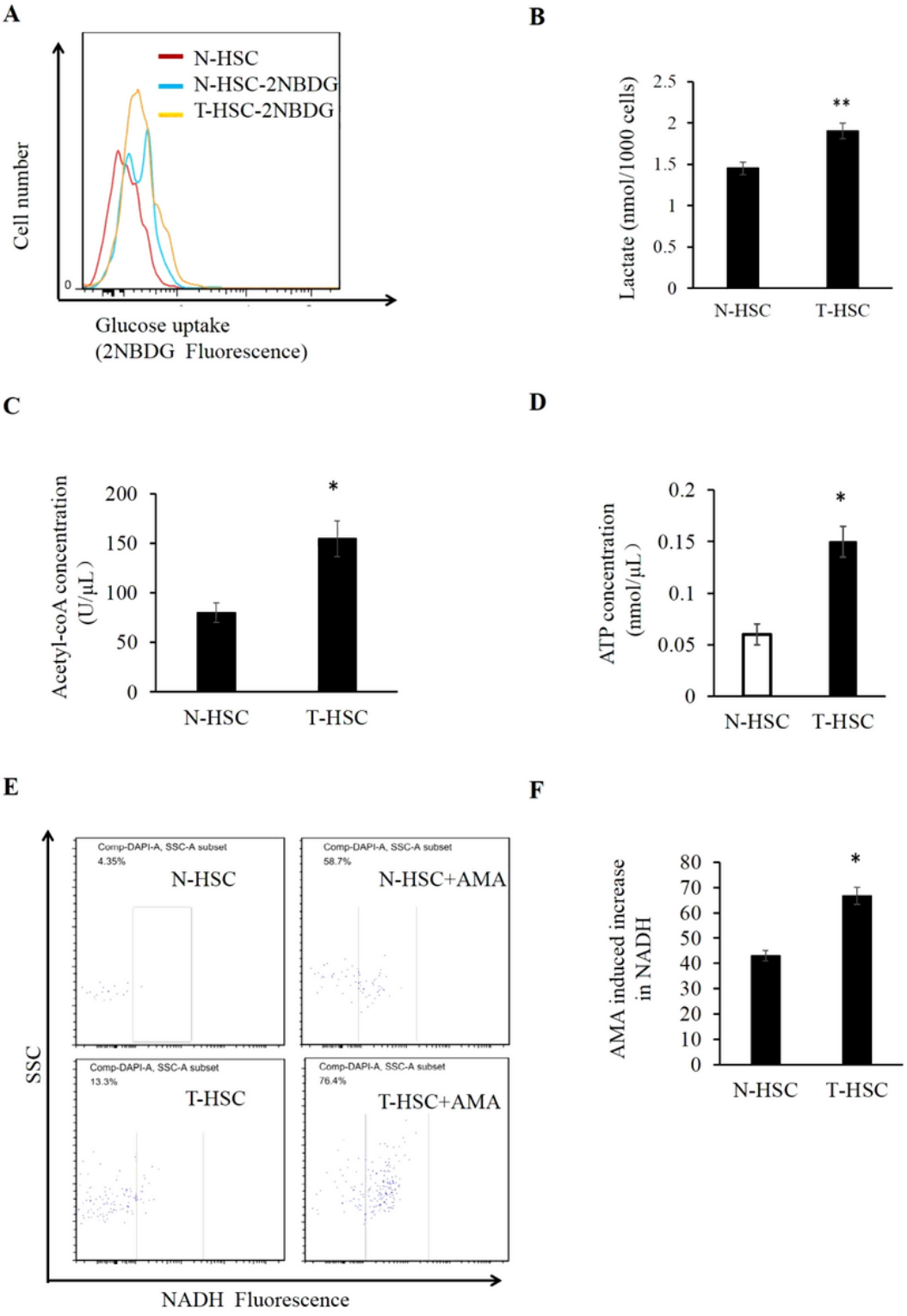

Figure 2

Changes in Glucose related metabolites in HSCs of Lung Cancer. (**A**) Representative plot of 2-NBDG fluorescence on N-HSCs and T-HSCs (mean-SD, n=3). (**B**) Lactate production in N-HSCs and T-HSCs per one thousand cells (mean ± SD, n=3; **p < 0.01). (**C**)Acetyl-CoA levels in N-HSCs and T-HSCs (mean ± SD, n=3; *p < 0.05). (**D**) Intracellular ATP concentration in N-HSCs and T-HSCs (mean ± SD, n=3; *p < 0.05). (**E**) Representative plot of cellular NADH: flow cytometry profiles ofcells before and after treatment with antimycin A (AMA). (mean ± SD, n=3; *p< 0.05).

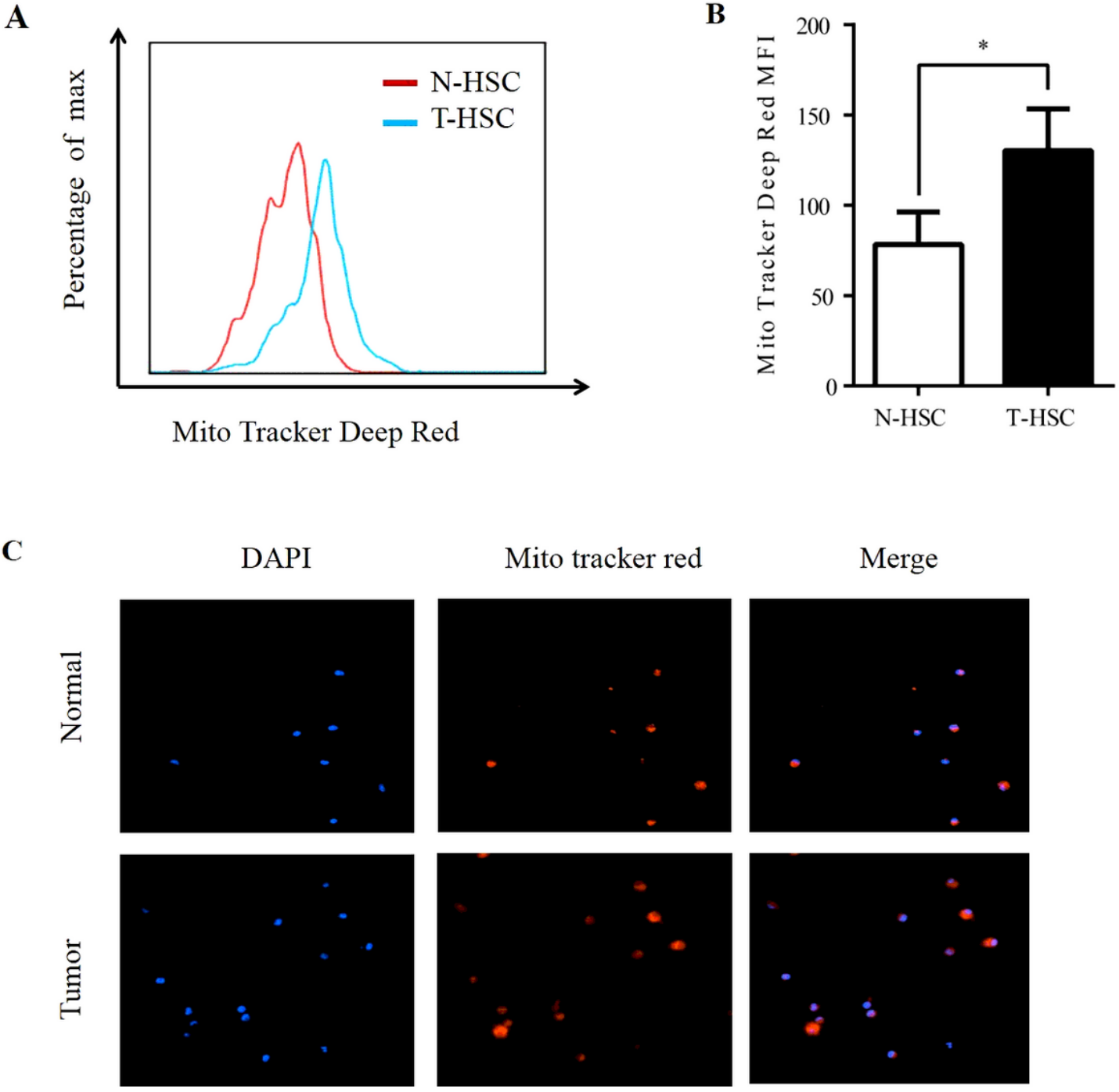

Figure 3

Changes in mitochondrial mass in HSCs by lung cancer. **(A)** Representative plot of Mito Tracker Deep Red staining on N-HSCs and T-HSCs analyzed by flow cytometry. **(B)** Quantitative analysis of Mito Tracker Deep Red median fluorescence intensity (MFI). (mean ± SD, n=5; *p < 0.05). **(C)** Immunocytochemical staining for mitochondrial dye Mito tracker Deep Red (red), and DAPI (blue) in N-HSCs and T-HSCs.

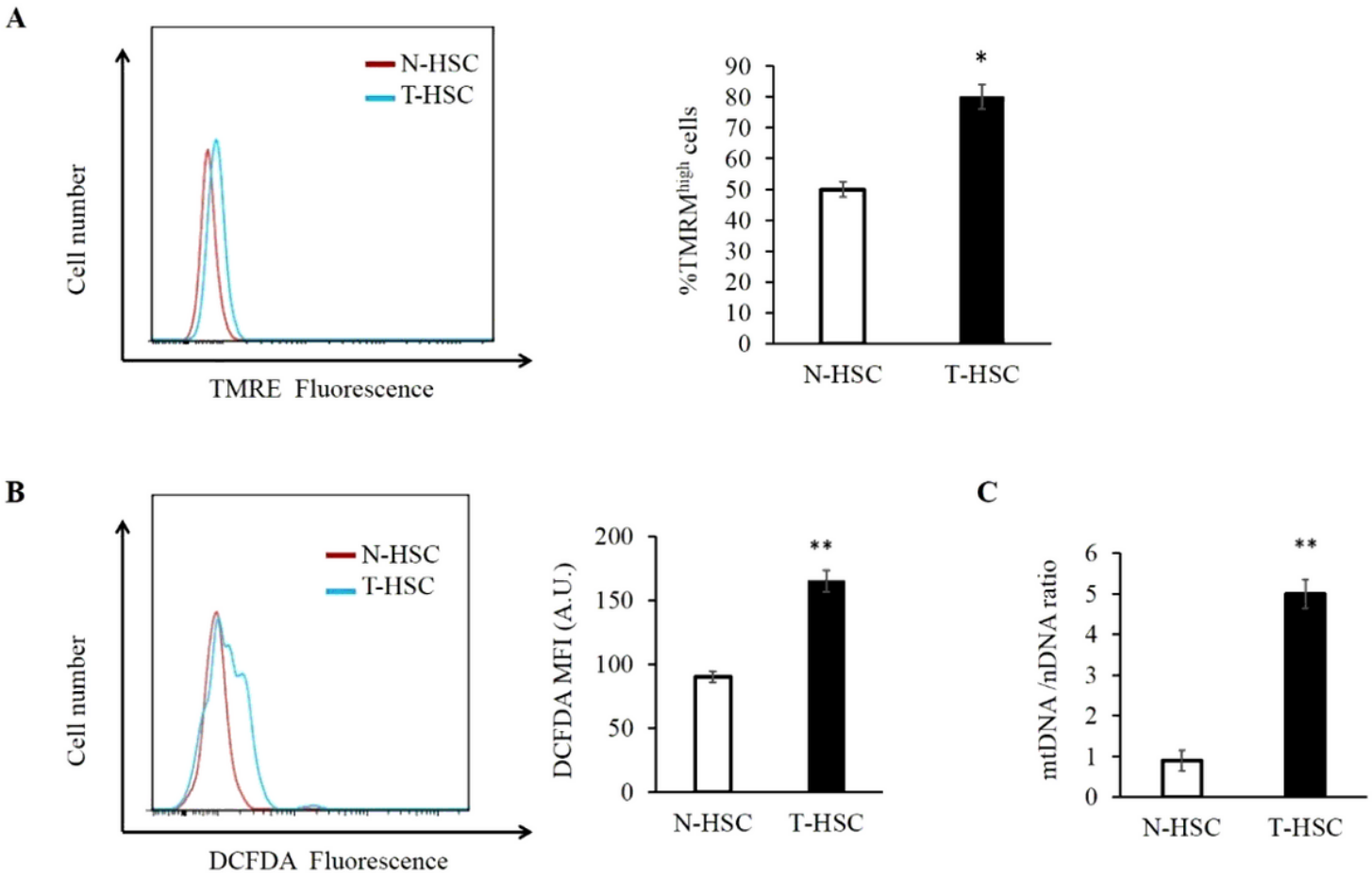

Figure 4

Impact of mitochondrial activity in lung cancer-conditioned HSCs. (**A**) (Left) Representative plot of tetramethylrhodamine methyl ester (TMRM) staining on N-HSCs and T-HSCs analyzed by flow cytometry. (Right) Quantitative analysis of cells that exhibit high levels of TMRM stain in N-HSCs and T-HSCs (mean ± SD, n=3 independent experiments; *p<0.05). (**B**) (Left) Representative plot of dichlorodihydro fluoresce in diacetate (DCFDA) staining on N-HSCs and T-HSCs analyzed by flow cytometry. (Right) Quantitative analysis of fold changes in DCFDA staining (mean ± SD, n=5 independent experiments; **p<0.01). (**C**) Quantitative analysis of mitochondrial DNA copy number relative to genomic DNA. (mean ± SD, n = 5; **p< 0.01)

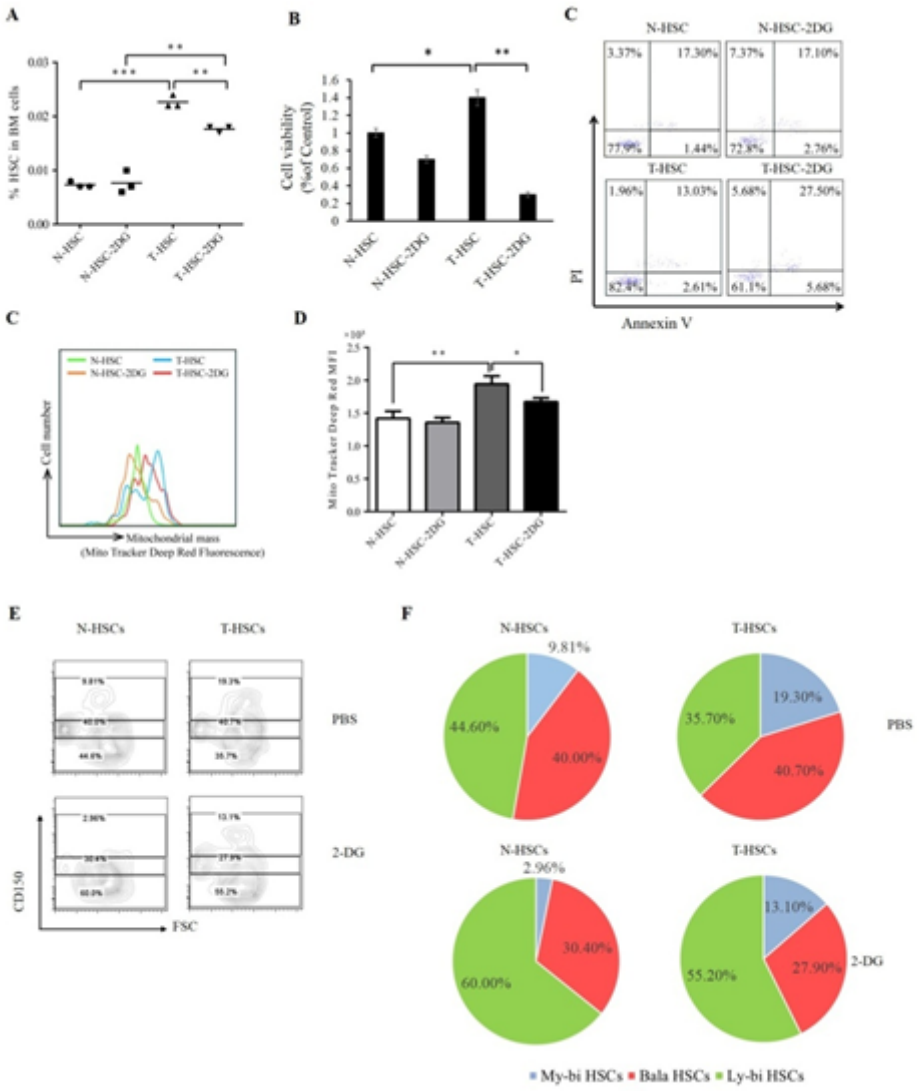

Figure 5

Changes in the function of T-HSCs after 2-DG stimulation. **(A)** Quantitative data on the percentages of N-HSCs and T-HSCs before and after treatment with 2-DG (mean ± SD, n = 3 independent experiments; *p < 0.05, **p< 0.01, ***p< 0.001). **(B)** Cell viability CCK8 of N-HSCs and T-HSCs before and after treatment with 2-DG assay (mean ± SD, n = 3 independent experiments; *p < 0.05, **p< 0.01). **(C)** Analysis on the apoptosis ratio of N-HSCs and T-HSCs before and after treatment with 2-DG (mean ± SD, n = 3 independent experiments; *p < 0.05, **p< 0.01). **(D)** Representative plot of Mito Tracker Deep Red staining on N-HSCs and T-HSCs before and after treatment with 2-DG analyzed by flow cytometry. **(E)** Quantitative analysis of Mito Tracker Deep Red median fluorescence intensity (MFI). (mean ± SD, n = 3 independent experiments; *p < 0.05, **p< 0.01). **(F)** Analysis of hematopoietic stem cell subtypes. Analysis of hematopoietic stem cell subtypes during tumorigenesis, and changes in hematopoietic stem cell subtypes before and after 2-DG stimulation. Myeloid biased HSCs (My-bi HSCs): $Lin^{-}Sca\text{-}1^{+}c\text{-}Kit^{+}CD34^{-}CD135^{-}CD150^{+}$; Balanced HSCs (Bala HSCs): $Lin^{-}Sca\text{-}1^{+}c\text{-}Kit^{+}CD34^{-}CD135^{-}CD150^{low}$; Lymphoid-biased HSCs (Ly-bi HSCs): $Lin^{-}Sca\text{-}1^{+}c\text{-}Kit^{+}CD34^{-}CD135^{-}CD150^{-}$.

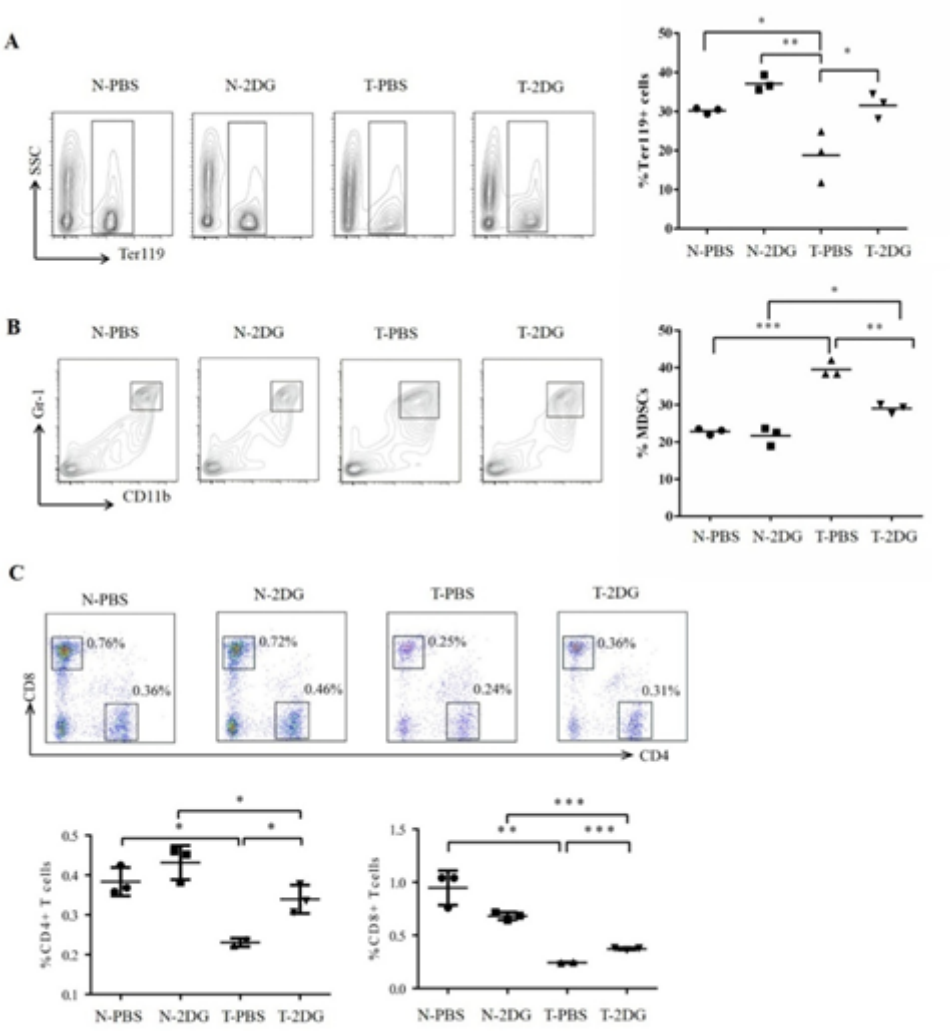

Figure 6

Changes in the content of immune cells in bone marrow after 2-DG stimulation. **(A)** Representative plot of the relative abundance of $Ter119^+$ cell in bone marrow before and after treatment with 2-DG analyzed by flow cytometry (Left). Quantitative data was shown on the right. (n = 3 independent experiments; ***p< 0.001, **p< 0.01, *p< 0.05). **(B)** Representative plot of the relative abundance of $Gr1^+CD11b^+$ cell in bone marrow before and after treatment with 2-DG analyzed by flow cytometry (Left). Quantitative data was shown on the right. (n = 3; ***p< 0.001, **p< 0.01, *p< 0.05). **(C)** Representative plot of the relative abundance of $CD4^+$ T cell and $CD8^+$ T cell in bone marrow before and after treatment with 2-DG analyzed by flow cytometry (Up). Quantitative data was shown below the plot. (n = 3 independent experiments ; ***p< 0.001, **p< 0.01, *p< 0.05).

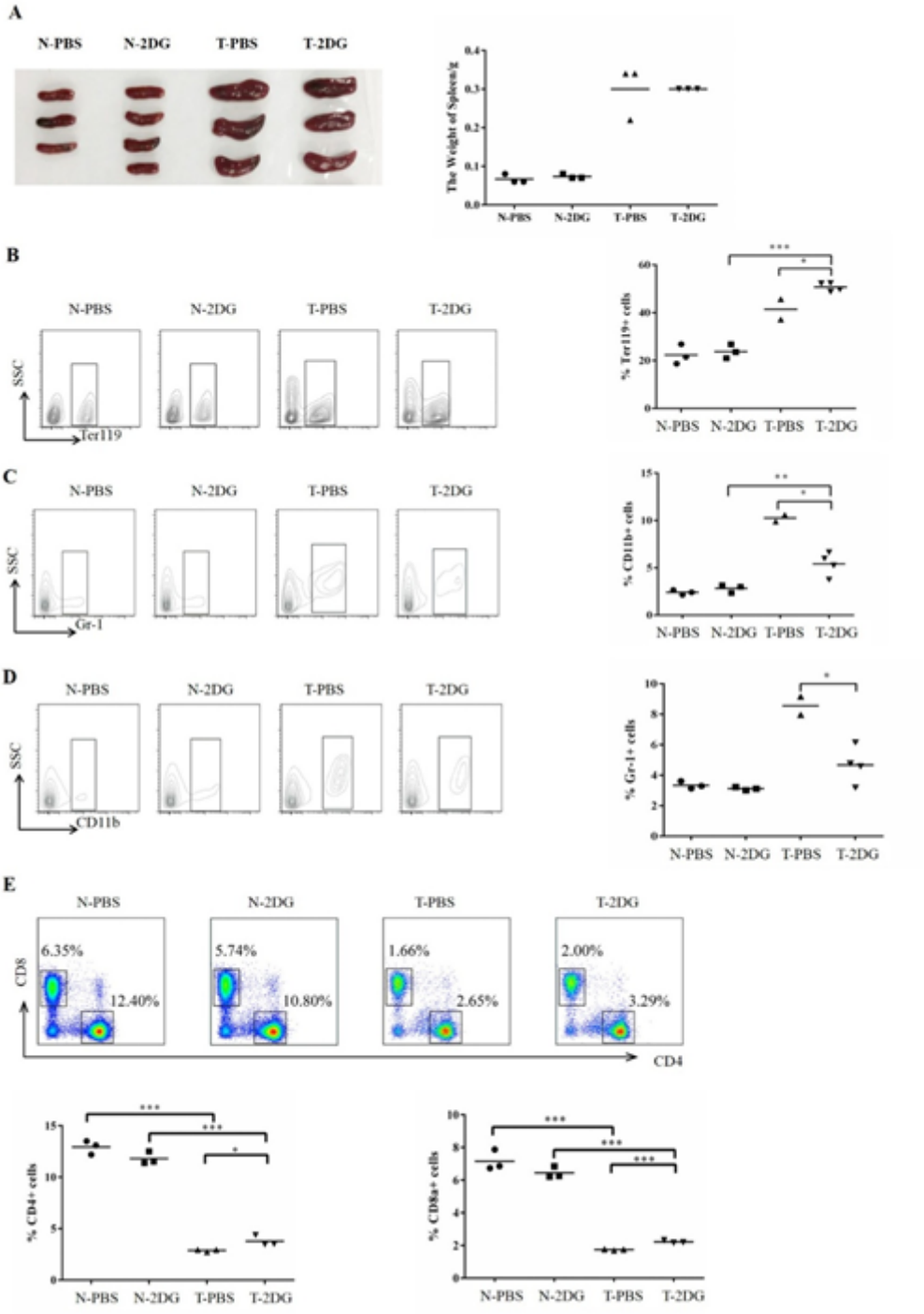

Figure 7

Changes in the content of immune cells in spleen after 2-DG stimulation. (A) Spleen size (Right) and weight (Left) of mice after 2-DG treatment. (B) Representative plot of the relative abundance of $Ter119^+$ cell in spleen before and after treatment with 2-DG analyzed by flow cytometry (Left). Quantitative data was shown on the right. (n=3; ***p< 0.001, **p< 0.01, *p< 0.05). (C) Representative plot of the relative abundance of $CD11b^+$ cell in bone marrow before and after treatment with 2-DG analyzed by flow cytometry (Left). Quantitative data was shown on the right. (n=3 independent experiments; ***p< 0.001, **p< 0.01, *p< 0.05). (D) Representative plot of the relative abundance of $Gr1^+$ cell in bone marrow before

and after treatment with 2-DG analyzed by flow cytometry (Left). Quantitative data was shown on the right. (n=3 independent experiments; ***p< 0.001, **p< 0.01, *p< 0.05). (E) Representative plot of the relative abundance of $CD4^+$ T cell and $CD8^+$ T cell in bone marrow before and after treatment with 2-DG analyzed by flow cytometry (Up). Quantitative data was shown below the plot. (n=3; *** p< 0.001, **p< 0.01, *p< 0.05).

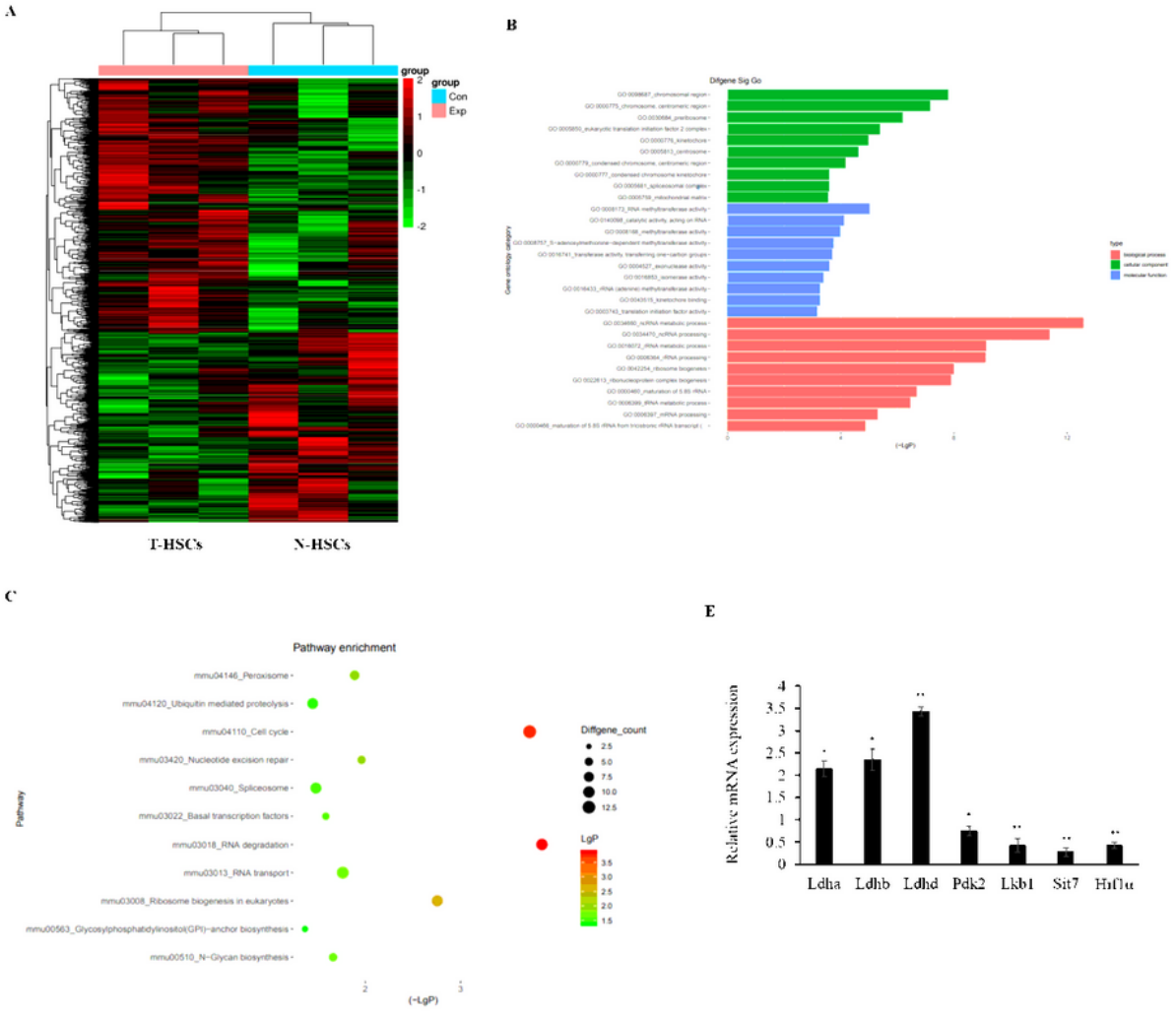

D

Gene_Accession	symbol	Gene_Description	Fold	diffState
NM_009038	Revrn	recoverin	5.27	up
NM_001161420	Vldlr	very low density lipoprotein receptor	4.12	up
XM_011239917	Gm21994	predicted gene 21994	3.39	up
NM_008152	Gpr65	G-protein coupled receptor 65	3.18	up
NM_181315	Car5b	carbonic anhydrase 5b, mitochondrial	2.85	up
NM_021396	Pdcd1lg2	programmed cell death 1 ligand 2	2.49	up
NM_009899	Clca3a1	chloride channel accessory 3A1	2.59	up
NM_011347	Selp	selectin, platelet	2.58	up
NM_013748	Clnk	cytokine-dependent hematopoietic cell linker	2.48	up
NM_183264	Tespa1	thymocyte expressed, positive selection associated 1	2.50	up
NM_181596	Retnlg	resistin like gamma	0.21	down
NM_013599	Mmp9	matrix metallopeptidase 9	0.20	down
NM_007895	Ear2	eosinophil-associated, ribonuclease A family, member 2	0.20	down
NM_001310438	Ly6g	lymphocyte antigen 6 complex, locus G	0.18	down
XM_001477102	I830127L07Rik	RIKEN cDNA I830127L07 gene	0.18	down
NM_001173460	Sirpb1b	signal-regulatory protein beta 1B	0.18	down
NM_009139	Ccl6	chemokine (C-C motif) ligand 6	0.18	down
NM_152839	Jchain	immunoglobulin joining chain	0.17	down
NM_010824	Mpo	myeloperoxidase	0.15	down
NM_178372	Prss34	protease, serine 34	0.11	down
NM_008572	Mcpt8	mast cell protease 8	0.07	down

Figure 8

Identification of differentially expressed genes in N-HSCs and T-HSCs. (A) Heat map of gene expression changes of T-HSCs compared to N-HSCs (n=3). (B) GO functional analysis of differentially expressed genes. (C) KEGG pathway analysis of differentially expressed genes. (D) The top 20 differentially expressed genes in T-HSCs. (E) qPCR validation of glycolysis and OXPHOS-related genes.